IJE TRANSACTIONS C: Aspects Vol. 34, No. 6, (June 2021) 1505-1513

International Journal of Engineering

Journal Homepage: www.ije.ir

Electromagnetic Wave Absorption Properties of Barium Ferrite/Reduced Graphene Oxide Nanocomposites

M. Moslehi Niasar[a], M. J. Molaei*[b], A. Aghaei[a]

[a] *Materials and Energy Research Center, Karaj, Iran*
[b] *Faculty of Chemical and Materials Engineering, Shahrood University of Technology, Shahrood, Iran*

PAPER INFO

Paper history:
Received 19 September 2020
Received in revised form 26 January 2021
Accepted 05 April 2021

Keywords:
Barium Ferrite
Reduced Graphene Oxide
Magnetic Properties
Electromagnetic Wave Absorption

ABSTRACT

Reduced graphene oxide (rGO) and M-type hexagonal ferrites such as $BaFe_{12}O_{19}$ have attracted great attention as electromagnetic (EM) wave absorbing materials in recent years. In this research, different weight percents of $BaFe_{12}O_{19}$/rGO nanocomposites were incorporated into the microwave absorbing layers and their EM wave absorption was investigated. Barium ferrite was synthesized through the co-precipitation method. Graphene oxide (GO) was synthesized through the modified Hummers' method. The synthesized GO was reduced to rGO nanosheets using a reducing agent. The synthesized barium ferrite and rGO were then mechanically milled to form $BaFe_{12}O_{19}$/rGO nanocomposite. The chemical bondings, phase analysis, magnetic properties, particle morphology, and EM wave absorbing properties were investigated using FTIR, XRD, Vibration Sample Magnetometer (VSM), FESEM, and Vector Network Analyzer (VNA), respectively. The saturation magnetization (M_s) and the coercivity (H_c) of the synthesized $BaFe_{12}O_{19}$/rGO nanocomposite were 31 emu/g and 1.5 kOe, respectively. The EM absorption properties in the X-band (8.2-12.4 GHz) showed that the maximum reflection loss (RL) of -7.39 dB could be obtained for the nanocomposite containing only 10 wt. % of $BaFe_{12}O_{19}$/rGO nanocomposite in a resin matrix with a thickness of 2 mm.

***doi**: 10.5829/ije.2021.34.06c.14*

1. INTRODUCTION

In recent years, electronic devices and wireless communications which act in the range of microwave frequency or X-band (8-12 GHz) are widely developed [1]. With the development of electronic devices, electromagnetic interference (EMI) has become a serious concern. Furthermore, the improvements in the technology of radar detection have increased the demand for microwave absorbing layers [2]. The microwave absorbing materials should be able to attenuate and dissipate the microwave energy through dielectric loss and magnetic loss mechanisms [1]. An ideal absorbing material should possess a broad absorption frequency, strong absorption capability, and lightweight [3]. The basic design criteria for the absorbing materials are impedance matching characteristics and attenuation capability [4, 5]. Generally, weak attenuation leads to a low reflection loss. Furthermore, weak impedance matching results in an increased reflection from the surface [5].

Most of the microwave absorbing materials have consisted of dielectric loss components such as conducting polymers or carbon material and magnetic loss materials such as nickel, cobalt, and ferrite [6]. Hexagonal ferrites with the chemical formula of $MFe_{12}O_{19}$ (M= Ba, Pb, and Sr) are the widely used hard magnetic materials in different applications [7]. Barium ferrite ($BaFe_{12}O_{19}$) as a hard magnetic material with enhanced saturation magnetization (M_s) and high coercivity (H_c) has received wide applications [8-17]. Barium ferrite has EM wave absorption properties as well [18]. However, due to the low dielectric loss and high density, the EM absorbing applications of hexagonal ferrites are restricted. In order to enhance the EM absorbing properties of hexagonal ferrites, versatile

*Corresponding Author Institutional Email: *m.molaei@shahroodut.ac.ir* (M. J. Molaei)

Please cite this article as: M. Moslehi Niasar, M. J. Molaei, A. Aghaei, Electromagnetic Wave Absorption Properties of Barium Ferrite/Reduced Graphene Oxide Nanocomposites, International Journal of Engineering, Transactions C: Aspects Vol. 34, No. 6, (2021) 1505-1513

dielectric loss fillers such as carbon nanotubes (CNTs) and graphene have been applied together with these ferrites [19].

Carbon-based materials such as CNTs, porous carbon, carbon spheres, graphene, and rGO have superior electromagnetic wave reflection loss efficiency. The rGO with a high dielectric loss is a great candidate for use in EM wave absorber materials [20]. Graphene, a monolayer sheet of carbon atoms in the form of a hexagonal two-dimensional structure with sp^2 hybridization, has attracted extensive attention due to its mechanical, electrical, and thermal properties. Graphene-based materials provide application potential in the fields of biomedical, supercapacitors, energy, catalysts, batteries, and EM wave absorption [21-23]. The graphene absorption properties can be enhanced if are used with other appropriate EM absorbing materials [24]. The graphene can act as a dielectric loss EM wave absorption material with an absorption performance better than CNTs [25]. The residual groups and defects on the rGO nanosheets introduce groups' electronic dipole relaxation and defect polarization relaxation. The rGO nanosheets have higher microwave absorption in comparison to CNT or graphite. The rGO nanosheets can also be a better microwave absorbing material compared to high-quality graphene [3]. However, graphene cannot be used as an appropriate microwave absorption material since it has a high dielectric loss while misses to have a high magnetic loss. In order to overcome this shortage, magnetic materials can be incorporated into graphene [26]. There have been some efforts to incorporate magnetic materials into rGO for enhancement of EM wave absorption properties including rGO/Fe_3O_4 [27], rGO/α-Fe_2O_3 [28], rGO/γ-Fe_2O_3 [29], rGO/$MnFe_2O_4$ [30], rGO/$ZnFe_2O_4$ [26], rGO/$CoFe_2O_4$ [31], rGO/Co_3O_4 [32], rGO/nitrogen-doped cobalt/cobalt oxide/carbon [33], rGO/Co_3Ni [34], rGO/ferroferric oxide-carbon [35], rGO/ hybrid C@CoFe nanoparticles [36].

While different magnetic materials have been used to enhance the microwave absorption properties of the rGO, barium ferrite as an effective microwave absorbing magnetic material, with different weight percents has not been used together with rGO to enhance the microwave absorption. Therefore, in this research, different weight percents of $BaFe_{12}O_{19}$/rGO nanocomposites were incorporated into a microwave absorbing layer, and their EM wave absorption properties were investigated. The barium ferrite was synthesized through the co-precipitation method while rGO nanosheets were synthesized by reduction of graphene oxide with hydrazine hydrate.

2. EXPERIMENTAL PROCEDURE

2. 1. Materials Graphite powder (purity 99.3%), hydrochloric acid (HCl, 10%), sulfuric acid (H_2SO_4, 98%), sodium nitrate ($NaNO_3$), potassium permanganate ($KMnO_4$), hydrogen peroxide (H_2O_2, 30%), ferric chloride ($FeCl_3.6H_2O$), barium chloride ($BaCl_2.2H_2O$), sodium hydroxide (NaOH), cetyltrimethyl ammonium bromide ($C_{19}H_{42}BrN$), and hydrazine hydrate ($NH_2NH_2 \cdot xH_2O$, 98%) were purchased from Merck. The epoxy (viscosity=1.75 MPa.s and density =1150 kg/m^3 at room temperature) and the hardener (viscosity=1.1 MPa.s and density=1000 kg/m^3 at room temperature) were also purchased from Shell company. All materials were reagent grade and were used without any further purification process.

2. 2. Synthesis of Barium Ferrite For the production of barium ferrite nanoparticles, $FeCl_3.6H_2O$ and $BaCl_2.2H_2O$ were added to 50 mL deionized water in a manner to reach to Fe:Ba molar ratio of 10. The cetyltrimethyl ammonium bromide (CTAB) surfactant was added (10 ppm) to decrease the agglomeration of the precipitates. The solution was stirred for 30 min. Then sodium hydroxide (5 M) solution added dropwise in 1 h to reach the pH of 11. During the addition of the sodium hydroxide, the ferrite precursors precipitate. The precipitates then were collected and washed using a 4000 rpm centrifuge and dried at 100 ◦C overnight. The dried precursors (reddish solids) were calcined at 1150 ◦C for 2 h in air.

2. 3. Synthesis of rGO Synthesis of rGO was conducted through chemical reduction of GO. The GO was synthesized by a modified Hummers' method [23]. Briefly, graphite (1 g) and $NaNO_3$ (2 g) were added into a flask containing H_2SO_4 (80 mL) and after stirring for 1 h, the mixture was transferred to an ice bath. Then $KMnO_4$ (3 g) was added to the flask under vigorous stirring. Subsequently, after continuous stirring for 48 h at room temperature, deionized water (400 mL) and H_2O_2 (15 mL) were added to the flask. The precipitate was washed with HCl (10%) and then with water to reach to pH of almost 7. The precipitate was dried at 80ºC in an oven overnight. Part of the resultant GO (0.4 g) was dissolved in deionized water (50 mL) using an ultrasonic bath. The GO was reduced to rGO with the aid of hydrazine hydrate (0.5 mL) under stirring for 1 h. The resultant rGO was collected and washed with deionized water for several times using an 11000 rpm centrifuge.

2. 3. Synthesis of $BaFe_{12}O_{19}$/rGO Nanocomposites The $BaFe_{12}O_{19}$/rGO nanocomposites were synthesized using a high energy mechanical milling. The weight ratio of the barium ferrite to rGO was 60/40. The powder mixtures were milled for 1 h in a SPEX-8000D milling machine with a ball to powder mass ratio of 7:1.

2. 4. Characterization Techniques Phase analysis was done using a Siemens model D500 XRD

machine. The XRD patterns were obtained with a step size of 0.02 degrees using Cu-K_α radiation. The analysis was completed with the help of X'pert software. Scherrer's equation [37] was used to calculate the mean crystallite size of the phases. Fourier-transform infrared spectroscopy (FTIR) analysis was performed on a PerkinElmer spectrometer (400-4000 cm^{-1}). The particle morphology was studied by a field emission scanning electron microscope (MIRA3TESCAN-XMU). Magnetic hysteresis loops of the samples were obtained by a vibrating sample magnetometer (VSM, Meghnatis Daghigh Kavir) at room temperature. The magnetization at the maximum applied field of 1.5 kOe was considered as the saturation magnetization. The EM wave absorption properties of the synthesized nanocomposites were measured by a vector network analyzer device (VNA, HP Network Analyzer, USA, model 8720) in the frequency range of 8.2-12.4 GHz at room temperature. For VNA measurements, the samples were prepared with different weight ratios of barium ferrite/rGO nanocomposites to the epoxy resin by the aid of slow mechanical agitation. The samples were prepared in similar thicknesses. The contents and thicknesses of the samples are listed in Table 1.

3. RESULTS AND DISCUSSIONS

Figure 1 shows the XRD patterns of the synthesized GO and barium ferrite/rGO nanocomposite. As can be seen in Figure 1, A sharp diffraction peak at $2\theta=12^\circ$ is detected in the pattern (a) which reveals the formation of GO. The pattern (b) merely consists of barium ferrite peaks, which implies that the milling of rGO and barium ferrite phases does not result in chemical reactions and the formation of new phases [37]. The electronic structure of the graphene nanosheets is modified by the lattice defects and attached functional groups. The defects and functional groups are scattering centers that alter the electrical properties. The reduction of GO to rGO removes the bonded oxygen-containing functional groups and also atomic-scale lattice defects. Furthermore, the reduction process recovers the conjugated network of the graphitic lattice. These change in the structure of the graphene sheets recovers the conductivity of the graphene [38]. The mechanism of the formation of barium ferrite is based on two competing processes: indirectly via crystalline intermediates and directly from the amorphous precursors. However, the direct formation of barium ferrite happens at lower temperatures because of its lower activation energy compared to the indirect route which posses higher activation energy [39].

Figure 2 displays the FTIR spectrum of the $BaFe_{12}O_{19}$/rGO nanocomposite. The peaks that are observed at 590 cm^{-1}, 545 cm^{-1}, and 442 cm^{-1} could be assigned to the Fe-O stretching vibrations [40]. The hydroxyl and carboxyl groups of the GO are absent on the FTIR spectrum of the synthesized nanocomposite. The peaks at 2914 cm^{-1}, 2842 cm^{-1}, and 1570 cm^{-1} due to C-H stretching and C=C stretching is evidence of the restoration of the graphitic structure [19].

FESEM images of the rGO nanosheets and $BaFe_{12}O_{19}$/rGO nanocomposite are shown in Figure 3. As can be seen in Figure 3(a), the lamellar structure has been conserved even after the chemical reduction of the GO.

TABLE 1. weight ratios of ferrite/rGO to epoxy resin in the samples alongside sample thicknesses

Samples	Barium ferrite/rGO content in the samples (wt%)	Epoxy resin content in the samples (wt%)	Thickness
I	10%	90%	2mm
II	20%	80%	2mm

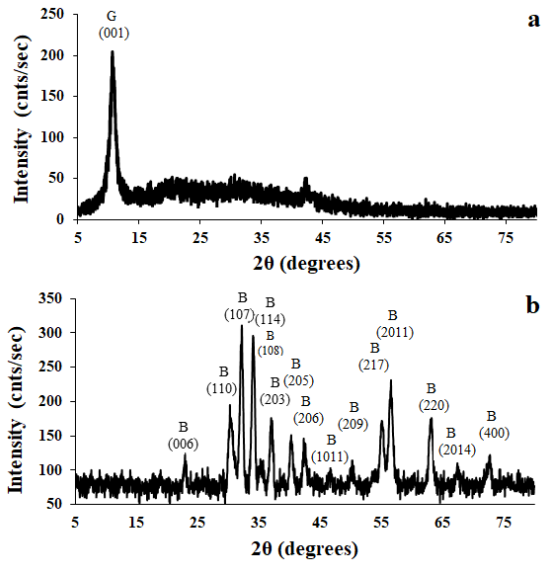

Figure 1. XRD patterns of the a) synthesized GO and b) $BaFe_{12}O_{19}$/rGO nanocomposite

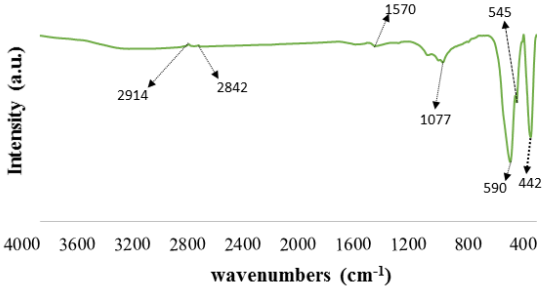

Figure 2. FTIR spectrum of $BaFe_{12}O_{19}$/rGO nanocomposite

Figure 3(b) shows rGO flakes that are decorated by barium ferrite nanoparticles which might have occurred due to an electrostatic attraction between rGO and $BaFe_{12}O_{19}$ [19].

Figure 4 shows the magnetic hysteresis loop of the synthesized $BaFe_{12}O_{19}$/rGO nanocomposites compared to barium ferrite. The nanocomposite of $BaFe_{12}O_{19}$ magnetic nanoparticles on the rGO flakes can reach a saturation magnetization (M_s) of 31 emu/g and coercivity (H_c) of 1.5 kOe.

Figure 5(a) shows the complex permittivity real part (ε′) and the imaginary part (ε″) of the $BaFe_{12}O_{19}$/rGO/epoxy nanocomposites with different weight ratios of $BaFe_{12}O_{19}$/rGO nanocomposite to epoxy at room temperature in the range of 8.2–12.4 GHz. It can be observed that the ε′ and ε″ values of the nanocomposites increased with an increase in the rGO content from 4 wt% to 8 wt%. Figure 5(b) shows the complex permeability real part (μ′) and the imaginary part (μ″) of the magnetic loss with different weight ratios of $BaFe_{12}O_{19}$/rGO nanocomposite to epoxy. The values of μ′ were in the range of 0.93–1.25 and the values of μ" were in the range of -0.03–0.25.

Considering the relative complex permeability which consists of real and imaginary parts, the real part (μ′) shows the storage capability and the imaginary part (μ″) represents the loss capability of the EM wave energy. The real and imaginary parts of permittivity (ε′ and ε″) also show energy storage and energy attenuation, respectively [30]. The values of ε′ and ε″ for the sample (Π) is high due to high conductivity. The chemical reduction of the graphene oxide results in an increase in the electrical conductivity and also dipolar induction. In fact, the relative complex permittivity is a measure of the polarizability [19]. The dielectric properties of the materials depend on ionic, electronic, space charge, interfacial, and orientational polarization. The sample with a higher content of rGO has enhanced conductivity and increased space charge polarization. The sample (Π) included more interfaces between rGO and barium ferrite nanoparticles that lead to more virtual charge accumulation at the interfaces. This results in interfacial polarization charges at the interface between phases with different dielectric constants. Therefore, the increased ε′ value is due to intrinsic dielectric properties and the increased ε″ value is due to enhanced space charge and interfacial polarization [41]. It is not advantageous for materials to have high values of permittivity since it may result in strong reflection and reduced absorption. On the other hand, for microwave absorbing properties low real part of permittivity and enhanced conductivity are preferred [42].

It can be seen in Figure 5(b) that the μ′ values show a slight increase by increasing the $BaFe_{12}O_{19}$/rGO content in the nanocomposites while μ″ values of the nanocomposite samples are almost unchanged. These

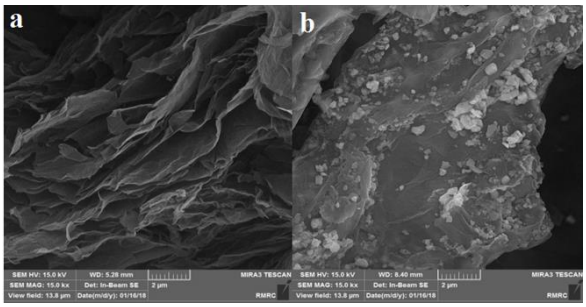

Figure 3. FESEM images of a) rGO flakes, b) rGO flakes decorated with barium ferrite nanoparticles

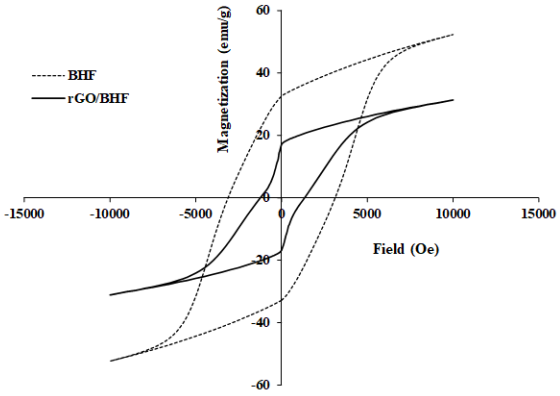

Figure 4. Magnetic hysteresis loop of pure $BaFe_{12}O_{19}$ (BHF) compared to $BaFe_{12}O_{19}$/rGO nanocomposite

data mean that the magnetic loss performance of the samples is nearly unchanged while the ability of the storage of the magnetic energy for the nanocomposites improves by increasing the $BaFe_{12}O_{19}$/rGO content.

The dielectric loss tangent ($\tan\delta_\varepsilon = \varepsilon''/\varepsilon'$) and the magnetic loss tangent ($\tan\delta_\mu = \mu''/\mu'$) variations of the synthesized nanocomposites in the measured frequency range are calculated and plotted in Figure 6. It can be seen in Figure 6(a) that $\tan\delta_\varepsilon$ values $BaFe_{12}O_{19}$/rGO/epoxy nanocomposites of the sample (Π) are higher than that of the sample (I). The higher values of $\tan\delta_\varepsilon$ in the sample with higher rGO content might be due to a) increased polarization as a result of surface functional groups which leads to higher dielectric loss and b) the role of rGO in contracting more conductive paths that result in higher dielectric loss [41]. As can be seen in Figure 6(b) both samples have nearly the same $\tan\delta_\mu$ curve that shows both samples have almost identical magnetic loss properties. Part of the dielectric loss is due to the conductivity loss and polarization loss. The electronic polarization and ionic polarization are significant in higher ranges of frequency (10^3–10^6 GHz) and are not considered for the current investigated frequency range [43]. The higher number of interfaces that exist between different phases in the sample with higher nanocomposite

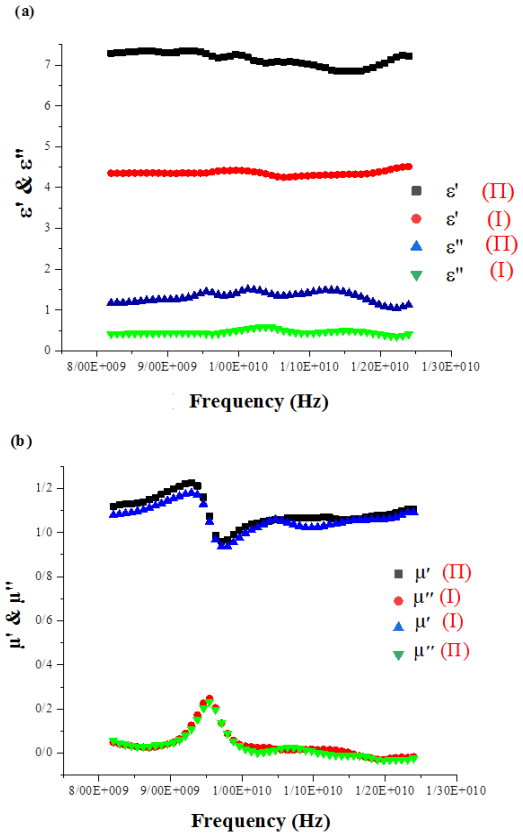

Figure 5. a) real and imaginary parts of the permittivity and b) real and imaginary parts of the permeability variations with different ratios of $BaFe_{12}O_{19}$/rGO nanocomposite to epoxy (samples I an II) in the range of 8.2-12.4 GHz

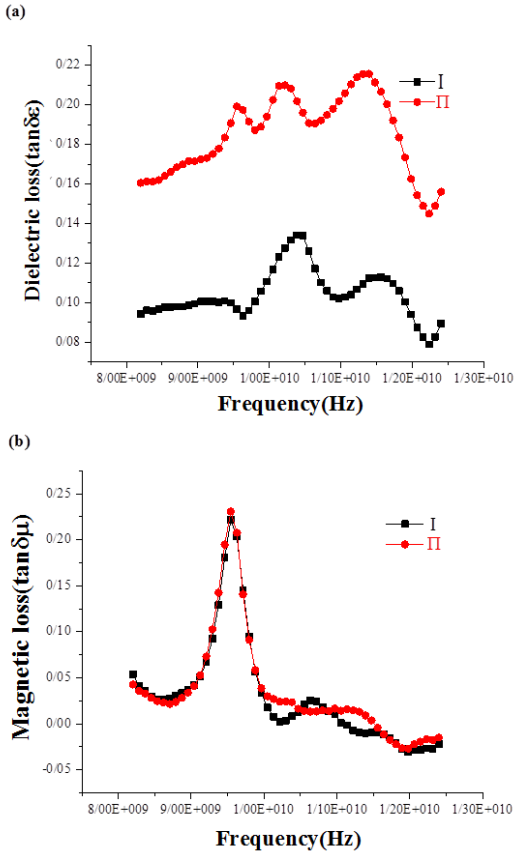

Figure 6. a) dielectric loss factor and b) magnetic loss factor of $BaFe_{12}O_{19}$/rGO/epoxy nanocomposites in the range of 8.2-12.4 GHz for the samples I and II

content, as well as charge transfer that can happen through $BaFe_{12}O_{19}$ nanoparticles and rGO interfaces, are responsible for the higher dielectric loss for sample II. These free carriers vibrate with stimuli of EM wave and cause electric polarization in the rGO [41].

A preferable $\tan\delta_e$ does not necessarily result in high absorption properties. There is another important criterion that should be satisfied for reaching a high microwave absorption efficiency. The characteristic impedance of the layer that is expected to absorb microwaves, should be equal or close to that of free space which is 377 Ωsq^{-1}. Under the impedance matching condition, the absorbing material will have zero-reflection of the incident EM wave at the front surface. For characteristic impedance matching, the complex permeability and complex permittivity should not differ greatly since in the case of large difference, the wave will reflect strongly at the surface of the absorbing material [44].

The reflection loss (RL) can be calculated by the following equation [20]:

$$RL(db) = 20\log\left|\frac{Z_{in}-Z_0}{Z_{in}+Z_0}\right| \quad (1)$$

where Z_0 is the impedance of air and Z_{in} is the input impedance at the interface between the absorber and air. This parameter is related to the EM parameters of the absorber material as follow [20]:

$$Z_{in} = Z_0\left(\frac{\mu_r}{\varepsilon_r}\right)^{\frac{1}{2}}\tanh\left\{j\left(\frac{2\pi ft}{c}\right)(\mu_r\varepsilon_r)^{\frac{1}{2}}\right\} \quad (2)$$

in which μ_r is complex permeability and ε_r is complex permittivity. The parameter c is the velocity of light in free space, *t* is the thickness of the absorbing sample, and *f* is the frequency.

In order to reach enhanced absorption, the incidence of the EM wave on the materials should be without front-end reflection and the EM wave should also be attenuated strongly during propagation in the material. The condition of impedance matching (Z_{in}/Z_0 =1) requires equal values of relative permittivity and permeability [45]. The calculated reflection loss of the $BaFe_{12}O_{19}$/rGO/epoxy nanocomposites with barium ferrite/rGO contents to epoxy weight ratios of 10% and 20% with the sample thicknesses of 2 mm, in the range of 8.2-12.4 GHz, is shown in Figure 7. The curves indicate that the maximum RL for the sample with

barium $BaFe_{12}O_{19}$/rGO content to epoxy of 20 wt% (sample Π) reaches 3.93 dB at 9.5 GHz. Furthermore, the RL of the sample with $BaFe_{12}O_{19}$/rGO content to epoxy of 10 wt% (sample I) reaches 7.39 dB at 9.5 GHz. It can be concluded from Figure 6 and RL data that the maximum absorption occurs at the frequency range in which $\tan\delta_\mu$ is higher than $\tan\delta_\varepsilon$ [45]. Table 2 summarizes microwave absorption of graphene-containing nanocomposites with different filling percents and thicknesses. The data in Table 2 shows that the $BaFe_{12}O_{19}$/rGO/epoxy resin nanocomposite synthesized in this research, shows better microwave absorption in low filling percent and thickness, compared to some other GO- and rGO-containing nanocomposites.

Figure 8 shows input impedance (Z_{in}) for the nanocomposite samples with respect to frequency. The blue curve reveals the conditions where the best impedance matching occurs. Impedance matching occurs when $Z_{in}/Z_0=1$. It can be seen in Figure 8 that the impedance matching in sample II is lower than that of sample I. This caused sample I to display better absorption performance rather than the other sample in all frequency ranges.

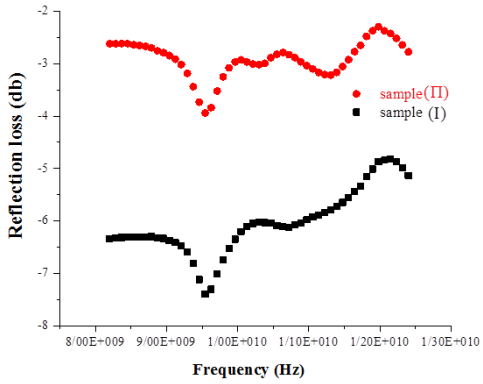

Figure 7. Reflectivity curves of $BaFe_{12}O_{19}$/rGO/epoxy nanocomposites with different barium ferrite/rGO contents to epoxy weight ratios

TABLE 2. Comparison of the microwave absorption of graphene-containing nanocomposites with different filling percents and thicknesses

Absorbing material	Filling percent	Thickness (mm)	Minimum reflection loss	Ref.
Functionalized rGO/γ-Fe_2O_3/Epoxy nanocomposite	60% wt	3	-10.2	[29]
Acid-imidazolium based dicationic ionic liquid (PTA@Imid diIL) interlocked on the surface of fluorinated GO/epoxy resin	20%	4	-5.8	[46]
Al@RGO/paraffin	60%	3	-7.7	[47]
Fe_3O_4-NH_2/GO nanocomposite	100%	4	-8	[48]

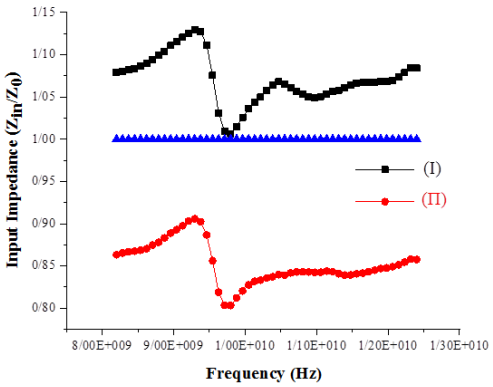

Figure 8. The impedance of $BaFe_{12}O_{19}$/rGO/epoxy nanocomposites in the range of 8.2-12.4 GHz for the samples I and Π

4. CONCLUSION

In this research, different contents of $BaFe_{12}O_{19}$/rGO nanocomposites were incorporated into epoxy resin and the microwave absorption properties of the absorbing layers were investigated.

Microstructural studies revealed a fine distribution of barium ferrite nanoparticles on the surface of rGO nanosheets forms through the coprecipitation method. The synthesized $BaFe_{12}O_{19}$/rGO nanocomposite was found to possess suitable magnetic properties (M_s=33 emu/g and H_c=2.1 kOe) to be used in EM wave absorption applications. The results of EM wave absorption measurements showed that the RL values of the $BaFe_{12}O_{19}$/rGO/epoxy nanocomposite are strongly influenced by their absorber material ratio in the sample. The sample with barium ferrite/rGO content of 10 wt% in the resin epoxy exhibits a maximum RL of 7.39 dB at 9.54 GHz. The results show that $BaFe_{12}O_{19}$/rGO nanocomposite is promising for the application in microwave absorbing layers.

5. ACKNOWLEDGMENT

The authors would like to acknowledge Materials and Energy Research Center, Shahrood University of Technology, and Iranian Nanotechnology Initiative Council for the financial support of present research.

6. REFERENCES

1. Widanarto, W., Khaeriyah, S., Ghoshal, S.K., Kurniawan, C., Effendi, M. and Cahyanto, W.T., "Selective microwave absorption in nd3+ substituted barium ferrite composites", ***Journal of Rare Earths***, Vol. 37, No. 12, (2019), 1320-1325, doi: 10.1016/j.jre.2019.01.008
2. Liu, C., Zhang, Y., Tang, Y., Wang, Z., Ma, N. and Du, P., "The tunable magnetic and microwave absorption properties of the Nb^{5+}–Ni^{2+} co-doped m-type barium ferrite", ***Journal of Materials Chemistry C***, Vol. 5, No. 14, (2017), 3461-3472, doi: 10.1039/C7TC00393E
3. Li, Y., Yu, M., Yang, P. and Fu, J., "Enhanced microwave absorption property of fe nanoparticles encapsulated within reduced graphene oxide with different thicknesses", ***Industrial & Engineering Chemistry Research***, Vol. 56, No. 31, (2017), 8872-8879, doi: 10.1021/acs.iecr.7b01732
4. Lv, H., Ji, G., Liang, X., Zhang, H. and Du, Y., "A novel rod-like MnO_2@ Fe loading on graphene giving excellent electromagnetic absorption properties", ***Journal of Materials Chemistry C***, Vol. 3, No. 19, (2015), 5056-5064, doi: 10.1039/C5TC00525F
5. Zhang, X., Ji, G., Liu, W., Zhang, X., Gao, Q., Li, Y. and Du, Y., "A novel co/tio 2 nanocomposite derived from a metal–organic framework: Synthesis and efficient microwave absorption", ***Journal of Materials Chemistry C***, Vol. 4, No. 9, (2016), 1860-1870, doi: 10.1039/C6TC00248J
6. Wang, C., Han, X., Xu, P., Zhang, X., Du, Y., Hu, S., Wang, J. and Wang, X., "The electromagnetic property of chemically reduced graphene oxide and its application as microwave absorbing material", ***Applied Physics Letters***, Vol. 98, No. 7, (2011), 072906, doi: 10.1063/1.3555436
7. Singhal, S., Garg, A. and Chandra, K., "Evolution of the magnetic properties during the thermal treatment of nanosize bamfe11o19 (m= Fe, Co, Ni and Al) obtained through aerosol route", ***Journal of Magnetism and Magnetic Materials***, Vol. 285, No. 1-2, (2005), 193-198, doi: 10.1016/j.jmmm.2004.07.039
8. Molaei, M., Ataie, A. and Raygan, S., "Synthesis of barium hexaferrite/iron oxides magnetic nano-composites via high energy ball milling and subsequent heat treatment", in International Journal of Modern Physics: Conference Series, World Scientific. Vol. 5, (2012), 519-526, doi: 10.1142/S2010194512002425
9. Molaei, M., Ataie, A. and Raygan, S., "Synthesis of magnetic nano-composite by partial reduction of barium hexaferrite via high-energy ball milling", in Key Engineering Materials, Trans Tech Publ. Vol. 434, (2010), 354-356, doi: 10.4028/www.scientific.net/KEM.434-435.354
10. Molaei, M., Ataie, A., Raygan, S., Picken, S. and Tichelaar, F., "Investigation on the effects of milling atmosphere on synthesis of barium ferrite/magnetite nanocomposite", ***Journal of Superconductivity and Novel Magnetism***, Vol. 25, No. 2, (2012), 519-524, doi: 10.1007/s10948-011-1322-2
11. Molaei, M., Ataie, A., Raygan, S. and Picken, S., "Role of intensive milling in the processing of barium ferrite/magnetite/iron hybrid magnetic nano-composites via partial reduction of barium ferrite", ***Materials Characterization***, Vol. 101, (2015), 78-82, doi: 10.1016/j.matchar.2015.01.006
12. Molaei, M., Ataie, A., Raygan, S., Picken, S. and Tichelaar, F., "The effect of heat treatment and re-calcination on magnetic properties of bafe12o19/Fe_3O_4 nano-composite", ***Ceramics International***, Vol. 38, No. 4, (2012), 3155-3159, doi: 10.1016/j.ceramint.2011.12.018
13. Molaei, M., Ataie, A., Raygan, S., Picken, S., Mendes, E. and Tichelaar, F., "Synthesis and characterization of bafe12o19/Fe_3O_4 and bafe12o19/Fe/Fe_3O_4 magnetic nano-composites", ***Powder Technology***, Vol. 221, (2012), 292-295, doi: 10.1016/j.powtec.2012.01.015
14. Molaei, M., Ataie, A., Raygan, S., Rahimipour, M., Picken, S., Tichelaar, F., Legarra, E. and Plazaola, F., "Magnetic property enhancement and characterization of nano-structured barium ferrite by mechano-thermal treatment", ***Materials Characterization***, Vol. 63, (2012), 83-89, doi: 10.1016/j.matchar.2011.11.004
15. Molaei, M., Ataie, A., Raygan, S. and Picken, S., "Exchange bias in barium ferrite/magnetite nanocomposites", ***Applied Physics A***, Vol. 123, No. 6, (2017), 437.
16. Molaei, M., Ataie, A., Raygan, S. and Picken, S., "The effect of different carbon reducing agents in synthesizing barium ferrite/magnetite nanocomposites", ***Materials Chemistry and Physics***, Vol. 219, No. 1, (2018), doi: 10.1016/j.matchemphys.2018.07.027
17. Zhang, Y., Chuyang L., Kangsen P., Yufan C., Gang F., and Yujing Z. "Synthesis of broad microwave absorption bandwidth Zr^{4+}-Ni^{2+} ions gradient-substituted barium ferrite." ***Ceramics International,*** Vol. 46, No. 16, (2020), 25808-25816, doi: 10.1016/j.ceramint.2020.07.062
18. Molaei, M. and Rahimipour, M., "Microwave reflection loss of magnetic/dielectric nanocomposites of bafe12o19/TiO_2", ***Materials Chemistry and Physics***, Vol. 167, (2015), 145-151, doi: 10.1016/j.matchemphys.2015.10.022
19. Verma, M., Singh, A.P., Sambyal, P., Singh, B.P., Dhawan, S. and Choudhary, V., "Barium ferrite decorated reduced graphene oxide nanocomposite for effective electromagnetic interference shielding", ***Physical Chemistry Chemical Physics***, Vol. 17, No. 3, (2015), 1610-1618, doi: 10.1039/C4CP04284K
20. Su, Z., Tan, L., Tao, J., Zhang, C., Yang, R. and Wen, F., "Enhanced microwave absorption properties of feni nanocrystals decorating reduced graphene oxide", ***Physica Status Solidi (b)***, (2018), 1700553, doi: 10.1002/pssb.201700553
21. Badiei, E., P. Sangpour, M. Bagheri, and M. Pazouki. "Graphene oxide antibacterial sheets: Synthesis and characterization (research note)." ***International Journal of Engineering, Transactions C: Aspects,*** Vol. 27, No. 12, (2014), 1803-1808, doi: 10.5829/idosi.ije.2014.27.12c.01
22. Allahyari, E., and M. Asgari. "Vibration Behavior of Nanocomposite Plate Reinforced by Pristine and Defective Graphene Sheets; an Analytical Approach." ***International Journal of Engineering, Transactions A: Basics,*** Vol. 31, No. 7 (2018), 1095-1102, doi: 10.5829/ije.2018.31.07a.13
23. Asemaneh, H. R., Laleh Rajabi, Farzad Dabirian, Neda Rostami, Ali Ashraf Derakhshan, and Reza Davarnejad. "Functionalized Graphene Oxide/Polyacrylonitrile Nanofibrous Composite: Pb^{2+} and Cd^{2+} Cations Adsorption." ***International Journal of Engineering, Transactions C: Aspects,*** Vol. 33, No. 6, (2020), 1048-1053, doi: 10.5829/ije.2020.33.06c.01
24. Durmus, Z., Durmus, A. and Kavas, H., "Synthesis and characterization of structural and magnetic properties of graphene/hard ferrite nanocomposites as microwave-absorbing material", ***Journal of Materials Science***, Vol. 50, No. 3, (2015), 1201-1213, doi: 10.1007/s10853-014-8676-3
25. Meng, F., Wang, H., Huang, F., Guo, Y., Wang, Z., Hui, D. and Zhou, Z., "Graphene-based microwave absorbing composites: A review and prospective", ***Composites Part B: Engineering***, Vol. 137, (2018), 260-277, doi: 10.1016/j.compositesb.2017.11.023
26. Yang, Z., Wan, Y., Xiong, G., Li, D., Li, Q., Ma, C., Guo, R. and Luo, H., "Facile synthesis of $ZnFe_2O_4$/reduced graphene oxide nanohybrids for enhanced microwave absorption properties", ***Materials Research Bulletin***, Vol. 61, (2015), 292-297, doi: 10.1016/j.materresbull.2014.10.004
27. Song, W.-L., Guan, X.-T., Fan, L.-Z., Cao, W.-Q., Zhao, Q.-L., Wang, C.-Y. and Cao, M.-S., "Tuning broadband microwave

absorption via highly conductive Fe_3O_4/graphene heterostructural nanofillers", ***Materials Research Bulletin***, Vol. 72, (2015), 316-323, doi: 10.1016/j.materresbull.2015.07.028

28. Chen, D., Wang, G.-S., He, S., Liu, J., Guo, L. and Cao, M.-S., "Controllable fabrication of mono-dispersed rgo–hematite nanocomposites and their enhanced wave absorption properties", ***Journal of Materials Chemistry A***, Vol. 1, No. 19, (2013), 5996-6003, doi: 10.1039/C3TA10664K
29. Jaiswal, R., Agarwal, K., Kumar, R., Kumar, R., Mukhopadhyay, K. and Prasad, N.E., "Emi and microwave absorbing efficiency of polyaniline-functionalized reduced graphene oxide/γ-Fe_2O_3/epoxy nanocomposite", ***Soft Matter***, Vol. 16, No. 28, (2020), 6643-6653, doi: 10.1039/D0SM00266F
30. Zhang, X.-J., Wang, G.-S., Cao, W.-Q., Wei, Y.-Z., Liang, J.-F., Guo, L. and Cao, M.-S., "Enhanced microwave absorption property of reduced graphene oxide (rgo)-$MnFe_2O_4$ nanocomposites and polyvinylidene fluoride", ***ACS Applied Materials & Interfaces***, Vol. 6, No. 10, (2014), 7471-7478, doi: 10.1021/am500862g
31. Zong, M., Huang, Y., Wu, H., Zhao, Y., Wang, Q. and Sun, X., "One-pot hydrothermal synthesis of rgo/$CoFe_2O_4$ composite and its excellent microwave absorption properties", ***Materials Letters***, Vol. 114, (2014), 52-55, doi: 10.1016/j.matlet.2013.09.113
32. Liu, P., Huang, Y., Wang, L., Zong, M. and Zhang, W., "Hydrothermal synthesis of reduced graphene oxide–Co_3O_4 composites and the excellent microwave electromagnetic properties", ***Materials Letters***, Vol. 107, (2013), 166-169, doi: 10.1016/j.matlet.2013.05.136
33. Shu, R., Wu, Y., Zhang, J., Wan, Z. and Li, X., "Facile synthesis of nitrogen-doped cobalt/cobalt oxide/carbon/reduced graphene oxide nanocomposites for electromagnetic wave absorption", ***Composites Part B: Engineering***, (2020), 108027, doi: 10.1016/j.compositesb.2020.108027
34. Guo, X., Bai, Z., Zhao, B., Zhang, R. and Chen, J., "Tailoring microwave-absorption properties of CoxNiy Alloy/rGO nanocomposites with tunable atomic ratios", ***Journal of Electronic Materials***, Vol. 46, No. 4, (2017), 2164-2171, doi: 10.1007/s11664-016-5152-7
35. Shu, R., Wu, Y., Li, W., Zhang, J., Liu, Y., Shi, J. and Zheng, M., "Fabrication of ferroferric oxide–carbon/reduced graphene oxide nanocomposites derived from Fe-based metal–organic frameworks for microwave absorption", ***Composites Science and Technology***, (2020), 108240, doi: 10.1016/j.compscitech.2020.108240
36. Li, J., Yang, S., Jiao, P., Peng, Q., Yin, W., Yuan, Y., Lu, H., He, X. and Li, Y., "Three-dimensional macroassembly of hybrid c@ cofe nanoparticles/reduced graphene oxide nanosheets towards multifunctional foam", ***Carbon***, Vol. 157, (2020), 427-436, doi: 10.1016/j.carbon.2019.10.074
37. Hakimi, M., Alimard, P. and Yousefi, M., "Green synthesis of reduced graphene oxide/Sr2CuMgFe28O46 nanocomposite with tunable magnetic properties", ***Ceramics International***, Vol. 40, No. 8, (2014), 11957-11961, doi: 10.1016/j.ceramint.2014.04.032
38. Pei, S. and Cheng, H.-M., "The reduction of graphene oxide", ***Carbon***, Vol. 50, No. 9, (2012), 3210-3228, doi: 10.1016/j.carbon.2011.11.010
39. Lisjak, D. and Drofenik, M., "The mechanism of the low-temperature formation of barium hexaferrite", ***Journal of the European Ceramic Society***, Vol. 27, No. 16, (2007), 4515-4520, doi: 10.1016/j.jeurceramsoc.2007.02.202
40. Ohlan, A., Singh, K., Chandra, A. and Dhawan, S.K., "Microwave absorption behavior of core− shell structured poly (3, 4-ethylenedioxy thiophene)− barium ferrite nanocomposites", ***ACS Applied Materials & Interfaces***, Vol. 2, No. 3, (2010), 927-933, doi: 10.1021/am900893d
41. Zhao, C., Shen, M., Li, Z., Sun, R., Xia, A. and Liu, X., "Green synthesis and enhanced microwave absorption property of reduced graphene oxide-SrFe12O19 nanocomposites", ***Journal of Alloys and Compounds***, Vol. 689, (2016), 1037-1043, doi: 10.1016/j.jallcom.2016.08.078
42. Wang, L., Huang, Y., Li, C., Chen, J. and Sun, X., "A facile one-pot method to synthesize a three-dimensional graphene@ carbon nanotube composite as a high-efficiency microwave absorber", ***Physical Chemistry Chemical Physics***, Vol. 17, No. 3, (2015), 2228-2234, doi: 10.1039/C4CP04745A
43. Zhou, C., Geng, S., Xu, X., Wang, T., Zhang, L., Tian, X., Yang, F., Yang, H. and Li, Y., "Lightweight hollow carbon nanospheres with tunable sizes towards enhancement in microwave absorption", ***Carbon***, Vol. 108, (2016), 234-241, doi: 10.1016/j.carbon.2016.07.015
44. Qiang, R., Du, Y., Wang, Y., Wang, N., Tian, C., Ma, J., Xu, P. and Han, X., "Rational design of yolk-shell c@ c microspheres for the effective enhancement in microwave absorption", ***Carbon***, Vol. 98, (2016), 599-606, doi: 10.1016/j.carbon.2015.11.054
45. Narang, S.B., Pubby, K. and Singh, C., "Thickness and composition tailoring of k-and ka-band microwave absorption of BaCoxTixFe12−2xO19 ferrites", ***Journal of Electronic Materials***, Vol. 46, No. 2, (2017), 718-728, doi: 10.1007/s11664-016-5059-3
46. Mohamadi, M., Kowsari, E., Yousefzadeh, M., Chinnappan, A. and Ramakrishna, S., "Highly-efficient microwave absorptivity in reduced graphene oxide modified with pta@ imidazolium based dicationic ionic liquid and fluorine atom", ***Composites Science and Technology***, Vol. 188, (2020), 107960, doi: 10.1016/j.compscitech.2019.107960
47. Fan, Q., Zhang, L., Xing, H., Wang, H. and Ji, X., "Microwave absorption and infrared stealth performance of reduced graphene oxide-wrapped al flake", ***Journal of Materials Science: Materials in Electronics***, Vol. 31, No. 4, (2020), 3005-3016, doi: 10.1007/s10854-019-02844-2
48. Ebrahimi-Tazangi, F., Hekmatara, S.H. and Seyed-Yazdi, J., "Synthesis and remarkable microwave absorption properties of amine-functionalized magnetite/graphene oxide nanocomposites", ***Journal of Alloys and Compounds***, Vol. 809, (2019), 151779, doi: 10.1016/j.jallcom.2019.151779

Persian Abstract

چکیده

فریت های هگزاگونال نوع M همانند $BaFe_{12}O_{19}$ ترکیبات فوق العاده ای در مواد جاذب امواج الکترومغناطیسی (EM) هستند. گرافن احیاء شده نیز یکی از مواد دو بعدی با جذب بالای امواج الکترومغناطیسی است. در این تحقیق خواص جذب امواج الکترومغناطیسی درصدهای وزنی مختلف از نانوکامپوزیت $BaFe_{12}O_{19}/rGO$ در لایه جاذب مایکروویو مورد استفاده بررسی قرار گرفت. هگزافریت باریم با استفاده از روش همرسوبی سنتز شد. اکسید گرافن (GO) با استفاده از روش هامرز سنتز شد. اکسید گرافن احیاء و به همراه هگزافریت باریم تحت آسیاکاری مکانیکی قرار گرفت. پیوندهای شیمیایی، آنالیز فازی، خواص مغناطیسی، مورفولوژی ذرات و خواص جذب مایکروویو به ترتیب با استفاده از طیف سنجی تبدیل فوریه مادون قرمز، پراش اشعه ایکس، مغناطش سنج نمونه مرتعش، میکروسکوپ الکترونی روبشی نشر میدانی و آنالایزر شبکه برداری مورد بررسی قرار گرفتند. تصاویر میکروسکوپ الکترونی روبشی نشان داد که نانوذرات هگزافریت باریم با موفقیت روی نانوصفحه های گرافن احیاء شده نشسته اند. مغناطش اشباع و نیروی پسماندزدا برای نانوکامپوزیت سنتز شده به ترتیب ۳۱ emu/g و ۱/۵ kOe بود. لایه جاذب امواج حاوی ۱۰٪ وزنی از نانوکامپوزیت $BaFe_{12}O_{19}/rGO$ در یک زمینه رزینی با ضخامت mm حداکثر اتلاف انعکاسی برابر ۷/۳۹ dB- در بازه X نشان داد.